The role of SWI sequence during the preoperative targeting of the subthalamic nucleus for deep brain stimulation in Parkinson's disease: A retrospective cohort study

Luigi Gianmaria Remore [a,b,*], Leonardo Tariciotti [a,b], Giorgio Fiore [a,b], Elena Pirola [a], Linda Borellini [c], Filippo Cogiamanian [c], Antonella Maria Ampollini [a], Luigi Schisano [a], Dario Gagliano [a,b], Stefano Borsa [a], Mauro Pluderi [a], Giulio Andrea Bertani [a], Sergio Barbieri [c], Marco Locatelli [a,d,e]

[a] Department of Neurosurgery, Fondazione IRCCS Ca'Granda Ospedale Maggiore Policlinico, Milan, Italy
[b] University of Milan LA STATALE, Milan, Italy
[c] Department of Neuropathophysiology, Fondazione IRCCS Ca'Granda Ospedale Maggiore Policlinico, Milan, Italy
[d] Department of Pathophysiology and Transplantation, University of Milan, Milan, Italy
[e] "Aldo Ravelli" Research Center for Neurotechnology and Experimental Brain Therapeutics, University of Milan, Milan, Italy

1. Introduction

Since the pioneering electrophysiologic studies by Benabid et al in 1987, deep brain stimulation (DBS) has been employed worldwide for the treatment of drug-resistant Parkinson's disease (PD) and the stimulation of the subthalamic nucleus (STN) was approved in 2002 by the FDA for patients with advanced PD.[1] The first method historically used to target STN is the so-called indirect targeting, which is based on specific anatomical landmarks (anterior and posterior commissures, midcommissural point) and classical stereotactic atlases such as the Schaltenbrand-Wahren brain atlas.[2] All the information collected from the aforementioned sources is then adapted to the single patient's anatomy to localize STN. This method is not patient-specific and may lead to under-expected results among different patients,[3] possibly because many atlases were designed on a limited and non-standardized population.[4] In this context, intraoperative MER is an invaluable tool to refine pre-operative indirect targeting by exploiting STN electrical activity in individual patients.[5] Despite the latter limitations, the indirect method is still used for the targeting of other brain structures, which are not well visualized with current MRI sequences.[6,7] On the other hand, direct targeting is based on the direct visualization of STN on a patient's MRI.[8] After the introduction of MRI and the advent of refined 3T MRI sequences, the direct targeting of the nucleus based on specific MRI sequences gained popularity among modern neurosurgeons.[9,10] In fact, it has been demonstrated that higher magnetic field-based MRI -such as 3T or even better 7T-allows finer visualization of STN.[11] The most commonly MRI sequences now employed for targeting are based on standard spin-echo (T1-weighted with gadolinium contrast,

T2-weighted), inversion recovery (FLAIR, fluid-attenuated inversion recovery) and susceptibility (T2*-weighted) techniques.[12] SWI (susceptibility-weighted imaging) is a susceptibility-based sequence, which is sensitive to the paramagnetic effects of iron-containing molecules.[13] This sequence is commonly employed in vascular neurosurgery as it is the most sensible in identifying and grading brain arteriovenous malformations.[14] The rationale for SWI application in STN-DBS for Parkinson's disease is justified by the continuous iron deposition in basal ganglia and deep cerebral nuclei as the neurodegenerative disease progresses.[15] In fact, SWI has been demonstrated to offer the highest contrast-to-noise ratio (CNR) in STN visualization with 3T brain MRI[4] and to better delineate the border between STN and SNr (substantia nigra pars reticulata).[16] Nevertheless, the effective clinical application of SWI in STN targeting is still a matter of debate and current evidence seems to contrast among different groups.[4,17–20]

Therefore, we performed a retrospective cohort study to investigate the advantages of adding the SWI sequence to the routine pre-operative MRI protocol for the targeting of STN.

2. Methods

2.1. Patients' selection and randomization

We reviewed the clinical database of our center for PD patients, who underwent STN-DBS from 2017 to 2020. 60 patients resulted from this search. All the PD patients selected for this study were screened by two expert attending neurologists (F.C. and L.B.) in the Movement Disorders Clinic at our institution and all surgical procedures were performed by the same attendant neurosurgeons (M.L. and E.P.) at the Neurosurgery Department of our institution. Both neurosurgeons had full training and great experience in stereotactic surgery and DBS procedures before the initial time point herein reported in this work. SWI sequence was introduced into our routine pre-surgical planning in 2019. In 15 patients implanted between 2019 and 2020, SWI sequence was used during preoperative planning. Then, we randomly chose 15 patients among the remaining 45 of our sample by using Research Randomizer software.[21] The former selected patients constituted the SWI-positive group, while the latter was the SWI-negative group. For each patient, three groups of variables were collected: personal data (gender, age at implantation, disease duration, first lateralized side affected by the disease), clinical data (calculated UPDRS III ON [with medications] and OFF [without medications] before and one year after the implantation; L-dopa dose assumed before and one year after the implantation) and electrophysiologic data (position of a second microelectrode for one or both sides during intraoperative recording if STN activity as recorded in the central lead was considered non-satisfying; choice of the central lead for definitive electrode implantation after intraoperative recording and stimulation of STN; mean length of intraoperative recording of STN activity). All patients gave informed written consent in accordance with the Declaration of Helsinki.

2.2. Electrodes reconstruction and localization

DBS electrodes were localized using the advanced processing pipeline[22] in Lead-DBS (Ver 2.5) (lead-dbs.org,[23]). As described in previous publications, postoperative CT was linearly co-registered to pre-operative MRI (T1-weighted with gadolinium contrast and T2-weighted sequences) using advanced normalization tools (ANTs; stnava.github.io/ANTs/,[24]). Co-registrations were inspected and refined when appropriate. Brain shift correction was applied as implemented in Lead-DBS. All preoperative volumes were used to estimate a precise multispectral normalization to ICBM 2009b NLIN asymmetric MNI space[25] applying the ANTs SyN Diffeomorphic Mapping[26] and using the preset "effective: low variance default + subcortical refinement". A multispectral implementation of the Unified Segmentation approach implemented in Statistical Parametric Mapping software (SPM12; fil.ion.ucl.ac.uk/spm,[27]) was applied when the previous approach failed. These two methods are available as presets in Lead-DBS and top-performed in segmenting the STN with as high precision as manually segmenting experts in a recent comparative study.[28] DBS contacts were automatically pre-reconstructed using the phantom-validated and fully automated PaCER method[29] or the TRAC/CORE approach and manually refined when appropriate. The resultant electrode models were then wrapped in the MNI space. Atlas segmentations in this manuscript are defined by the DISTAL atlas to visualize STN and its sensorimotor component.[30]

Group visualization and analysis of active contact location were performed using the Lead-Group tool in Lead-DBS.[22] By using this same software, we estimated the proper placement of the active contact into STN and its sensorimotor component as depicted by the DISTAL atlas with two methods. First, we calculated the rate of active contacts properly placed into the target nucleus by setting a 0.5 mm threshold, according to a standard threshold in Lead-Group as reported by other authors.[22] By doing so, only the active contacts whose center was not farther than 0.5 mm from the nearest voxel center of the nucleus would be considered correctly placed. Then, we also reported the millimetric distance from the active contact center to the nearest atlas voxel of the target nucleus.

2.3. Surgical procedure

The surgical procedure performed on all patients consisted of a two-step procedure as previously described.[31] Pre-operative MRI data were acquired on a 3T system (Achieva; Philips Medical System, Best, the Netherlands) by using a six-channel phased-array head coil. Each patient was scanned with our PD-DBS imaging protocol, which included T1-weighted with gadolinium contrast, T2-weighted, FLAIR, and T2*-weighted sequences. This same MRI protocol was adopted by our centers until 2019. The SWI sequence was added for the patients who underwent STN-DBS from 2019 onwards. SWI scanning parameters were acquired as follows: FOV = $230 \times 189 \times 130$ mm^3, reconstruction matrix = 512 (voxel size = $0.6 \times 0.6 \times 2$ mm^3), TEs (51, 9.8, 6.8 ms) with the corresponding shortest possible TRs of 48, 5.9, 6.5 ms respectively, acquisition time = 4.23 min. During preoperative planning, the attending neurosurgeons employed both SWI and other "canonical" MRI sequences (T2* and FLAIR) for STN targeting, while only T2* and FLAIR were used for STN targeting in SWI-negative group patients. For patients in the SWI-positive group specifically, the neurosurgeons first used SWI to identify STN-SNr borders on coronal and sagittal planes and then refined the target on the axial plane by also integrating the T2* and FLAIR sequences.

Before the surgery, a Cosman-Roberts-Wells stereotactic frame (Radionics [Integra, Plainsboro, New Jersey, USA]) was placed on the patient's head under local anesthesia and a stereotactic CT scan was performed. The CT was then combined with MRI sequences in a dedicated workstation (Istereotaxy, Brainlab, Kapellenstrat, Germany). In the first step, bilateral intracerebral leads were implanted under local anesthesia in the awake patient. The implantation site for the first lead was always contralateral to the more clinically affected side. Before lead implantation, recording microelectrodes (FHC. INC, Bowdoin, Maine, USA) were placed and the electrophysiologic activity of STN was tested. Possible side effects from intraoperative stimulation were then investigated by an attending neurologist of our dedicated movement disorder team. In the case of unclear electrophysiologic activity of the nucleus or severe side effects, a second lead was chosen and microelectrode recording was repeated. If both leads displayed similar side effects, the central lead or the one with the better nuclear activity was selected. After the correct electrophysiologic localization of the nucleus, definitive leads (Model 3389 [Medtronic Inc., Minneapolis, Minnesota, USA]) were implanted. A CT scan was performed on all patients at the end of the surgical procedure. The second step was performed under general anesthesia. During this surgical time, intracranial electrodes were

elongated with lead extenders, which were then connected to an IPG Medtronic Activa PC implanted into a subcutaneous pouch in the right hemithorax. This procedure was generally scheduled within 7 days after lead placement. Patients were subsequently discharged and the stimulation was turned on 3–6 weeks after surgery during a second hospitalization.

2.4. Statistical analysis

Descriptive statistics, frequencies and percentages were used to report demographic characteristics. A Shapiro–Wilk normality test was used to assess normality across selected variables. Continuous variables were reported as mean +standard deviation (SD) or median and interquartile range (IQR) when appropriate. Categorical variables were reported as absolute numbers and percentages (N%). Normal variables were reported as mean ± standard deviation (SD) and compared by Student *t*-test, skewed variables were reported as the median and interquartile range (IQR) and compared by Mann–Whitney *U* test. Categorical variables were reported as absolute "counts (percentages)" and intergroup comparison was computed using Mann–Whitney *U* test or Kruskall Wallis test whether the binary or multiclass comparison was investigated. Right and left active contacts were grouped and analyzed as a single variable (30 active contacts for 15 SWI-positive patients and 30 active contacts for 15 SWI-negative patients). Consequently, the active contact location was compared between the two groups. The same analysis was repeated for the millimetric distance of the active contact from STN. For all traditional hypotheses, *p* values < 0.05 were considered statistically significant. Statistical analysis was performed using SPSS (version 27.0, IBM).

3. Results

3.1. Demographic and clinical characteristics

When considering the whole group of 30 patients selected for this study, no differences were found in sex (50% male VS 50% female) and the bodyside first affected by the disease (50% left VS 50% right). The mean age at implantation was 58.83 ± 9.7 years and the mean duration of Parkinson's disease before DBS was 11.43 ± 4.15 years (Table 1). Before the implantation, the mean L-Dopa dosage assumed by patients was 881.2 ± 380 mg, while the mean UPDRS III ON and OFF were 17.83 ± 6.14 and 40.10 ± 10.24, respectively.

Comparing the two groups, patients in the SWI-positive group were more often males (SWI-positive: 66.7% VS SWI-negative: 33.3%; *p* = 0.07). The mean age at implantation was 60.67 ± 10.81 and 57 ± 8.41 years (*p* = 0.3) for the SWI-positive and SWI-negative groups, respectively. The mean duration of the disease before the surgical procedure was similar for both groups (12 ± 4 years for the SWI-positive group and 10.87 ± 4.37 years for the SWI-negative group; *p* = 0.46), whereas the bodyside first affected was the right and the left one for the SWI-positive and SWI-negative groups, respectively (SWI-positive: right 53.3% VS left 46.7%; SWI-negative: right 46.7% VS left 53.3%; *p* = 0.71). When considering the SWI-positive and the SWI-negative groups separately, the mean L-Dopa dosage assumed before the surgical procedure was 802.47 ± 385.7 mg in the former and 820 ± 387.71 mg in the latter (*p* = 0.9). Moreover, the two mean UPDRS III for the SWI-positive and SWI-negative groups were as follows: ON: 18.20 ± 7.2 VS 17.47 ± 5.14 (*p* = 0.75); OFF: 40 ± 11.68 VS 40.2 ± 9 (*p* = 0.95). One year after the implantation, the mean L-Dopa dosage was almost equivalent between the two groups (466 ± 150 VS 500 ± 250 mg, *p* = 0.6). However, SWI-positive patients had a lower score in both UPDRS III ON (13.67 ± 6.05 VS 17.06 ± 3.32, *p* = 0.067) and UPDRS III OFF (24.6 ± 8.7 VS 29.2 ± 5, *p* = 0.087) one year after the surgery (Table 2).

Table 1
Demographic and clinical characteristics of patients.

PATIENT	SWI[a]	SEX[b]	AGE[c]	DISEASE DURATION[d]	BODYSIDE FIRST AFFECTED
1	Yes	M	47	7	Left
2	Yes	M	63	13	Left
3	Yes	M	64	11	Right
4	Yes	M	58	14	Right
5	Yes	F	70	15	Right
6	Yes	M	55	7	Left
7	Yes	M	69	15	Right
8	Yes	F	60	8	Right
9	Yes	M	69	10	Left
10	Yes	M	65	9	Left
11	Yes	M	36	8	Right
12	Yes	F	44	11	Right
13	Yes	M	69	19	Right
14	Yes	F	71	19	Left
15	Yes	F	70	14	Left
16	No	M	42	15	Right
17	No	M	61	11	Right
18	No	M	56	14	Left
19	No	F	54	5	Left
20	No	M	61	5	Right
21	No	F	44	9	Right
22	No	F	47	8	Left
23	No	F	62	17	Right
24	No	F	58	18	Left
25	No	M	59	11	Left
26	No	F	51	9	Left
27	No	F	69	17	Left
28	No	F	68	7	Right
29	No	F	55	10	Left
30	No	F	68	7	Right

Notes: a: presence or absence of SWI sequence in the pre-operative MRI protocol for STN targeting; b: *M* = male, F = female; c: patient's age at the time of implantation, expressed in years; d: duration of Parkinson's disease before implantation, expressed in years.

3.2. Electrodes location in STN and electrophysiology

More frequently in the SWI-positive group than the SWI-negative group, the active contact of has resulted to be in STN (80% vs 66.7%, *p* = 0.243) and in its sensorimotor component (73.3% vs 32%, *p* = 0.018) (Fig. 1). These results were confirmed when comparing between the SWI-positive group and the SWI-negative group the mean distance of the active contact center from the whole STN (0.35 ± 0.53 mm VS 0.4 ± 0.5 mm, *p* = 0.38) and the sensorimotor subcomponent of STN (0.5 ± 0.77 mm VS 1.02 ± 0.81 mm, *p* = 0.028). A second microelectrode for one or both sides during intraoperative recording was placed more frequently for SWI-negative than SWI-positive patients if STN activity as recorded in the central lead was considered non-satisfying (86.7% vs 13.3% [*p* < 0.0001]). Furthermore, the mean length of intraoperative recording of STN activity was greater in the SWI-positive than in the SWI-negative group (SWI-positive: 8 ± 0.85 mm VS SWI-negative: 6.84 ± 1.51 mm [*p* = 0.013]), while the difference between the two groups was less relevant when considering the choice of the central lead for definitive electrode implantation (SWI-positive: 86.7% VS SWI-negative: 73.3% [*p* = 0.36]) (Table 2).

4. Discussion

Our study demonstrated more precise STN targeting when the SWI sequence is integrated into the preoperative MRI targeting protocol. The groups in this study were homogeneous, since no statistically significant differences were found in personal and clinical data among the patients before the surgery. The location of the active contacts in STN and its sensorimotor component as visualized in the DISTAL atlas was more frequent in patients for whom the preoperative STN targeting was conducted by implementing the standard radiological protocol with the

Table 2
Clinical and electrophysiologic variables for SWI-positive and SWI-negative group.

VARIABLES		SWI-POSITIVE GROUP	SWI-NEGATIVE GROUP	*p*-VALUE*
ELECTRODES	Electrode in STN[†]	80%	66.7%	0.243
	Electrode in smSTN[‡]	73.3%	32%	0.018
	Contact-STN distance[§]	0.35	0.4	0.38
	Contact-smSTN distance	0.5	1.02	0.028
ELECTROPHYSIOLOGY	Second recording lead[II]	85%	8%	<0.0001
	Central lead[¶]	92%	85%	0.54
	Recording length[#]	8	7	0.052
CLINICAL DATA	L-DOPA Pre**	802.47	820	0.9
	L-DOPA Post	466	500	0.6
	UPDRS III ON Pre***	18.20	17.47	0.75
	UPDRS III OFF Pre	40	40.2	0.95
	UPDRS III ON Post	13.67	17.06	0.067
	UPDRS III OFF Post	24.6	29.2	0.087

Notes: *: *p* values < 0.05 were considered statistically significant; †: position of electrode's active contact in the subthalamic (STN) nucleus; ‡: position of electrode's active contact in the sensorimotor portion of the subthalamic (sm-STN) nucleus; §: distance from the center of the active contact to the nearest voxel of the target nucleus as depicted in the DISTAL atlas; II: position of a second microelectrode for one or both sides during the intraoperative recording of STN activity; ¶: choice of the central lead for definitive electrode after intraoperative recording and stimulation of STN; #: mean length of intra-operative recording of STN activity in mm; **: mean levodopamine (L-DOPA) dose calculated before and one year after the implantation; ***: calculated mean UPDRS III ON (with medications) and OFF (without medications) before and after the implantation.

SWI sequence. This evidence resulted statistically significant (*p* = 0.018). Furthermore, our analysis showed a greater distance from the center of the active contact to the target nucleus in the SWI-negative than the SWI-positive groups. Even this finding reached statistical significance (*p* = 0.028). These results may appear in contradiction with the well-known nonlocal susceptibility effect, which is common to all susceptibility-based MRI sequences including SWI. Despite better visualization of STN because of its higher CNR, the not-uniformly distributed iron molecules within STN produce a local magnetic field in response to the magnetic field produced by the MRI scanner, which can extend beyond the actual border of STN and cause faster proton relaxation in the surrounding tissue. These so-called blooming artifacts may blur and overestimate STN borders,[12] as previously published by other authors.[19,20] However, McEvoy et al compared the radiological appearance of STN in T2-weighted and SWI sequences and reported better visualization of STN-SNr borders with SWI, especially in coronal and sagittal sections.[16] Moreover, the same group described the coincidence of the STN-SNr boundary detected by SWI with the change in electrical activity as recorded by intraoperative MER when trespassing the two nuclei. This finding is consistent with the results presented in our investigation: in fact, we found a statistically significant (*p* < 0.0001) less frequent placement of a second microelectrode for one or both sides during intraoperative recording in the SWI-positive than the
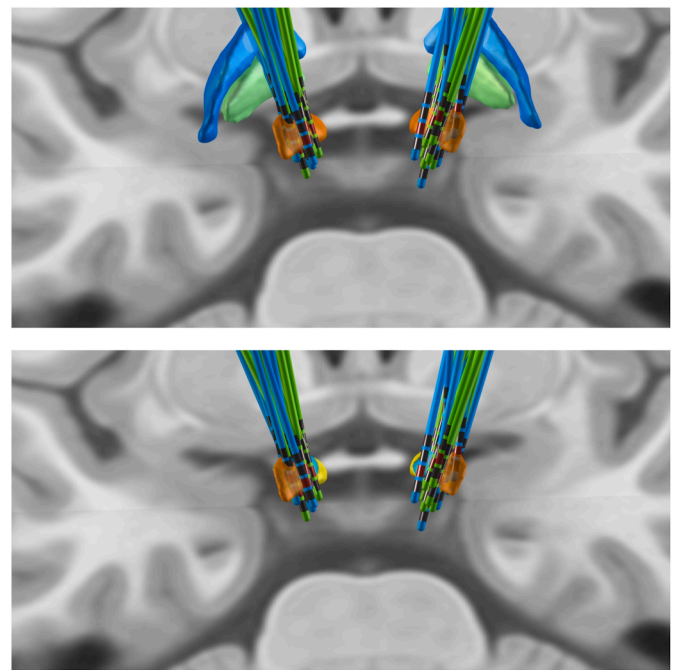

Fig. 1. Group-level reconstruction of patients' electrodes as rendered in Lead-DBS 3D viewer with the MNI ICBM 2009b NLIN ASYM T1 as background. Subcortical structures are identified according to DISTAL Atlas: subthalamic nucleus (orange), globus pallidum pars interna (green), globus pallidum pars externa (blue).
Upper image: patients' electrodes reconstruction as group-level and their position relative to the subthalamic nucleus. Electrodes from the SWI-positive group are colored in blue, while electrodes from the SWI-negative group are colored in green. Active contacts are enlightened in red.
Lower image: same reconstruction as above but focused on the subthalamic nucleus and its functional subcomponents: the sensorimotor part in orange, the associative part in light blue and the limbic part in yellow.

SWI-negative group. Furthermore, a slightly more frequent choice of the central registration lead for definitive electrode placement (*p* = 0.36) and statistically significant longer intraoperative recording of STN activity (*p* = 0.013) were evident in patients of the SWI-positive group. Overall, these results demonstrated the coincidence of the anatomical target identified preoperatively by adding the SWI sequence to the neuroimaging planning protocol with the activity of the STN nucleus as resulted by intra-operative electrophysiology, since SWI-positive patients had better intraoperative STN activity as evidenced by a longer mean length of the intraoperative recording and by a more frequent placement of the definitive electrode in the central position of the microguide– that corresponds to the anatomical target calculated pre-operatively and is the first lead to be tested with MER-, without the need of a second microelectrode in a different position due to a non-satisfying STN activity in the central lead.

Given so, we hypothesize that the main advantage of the SWI sequence might be the better localization of STN-SNr borders rather than the optimal visualization of STN per se. STN-SNr borders have an important electrophysiological meaning when looking for STN activity intraoperatively and may be used by the neurosurgeon as an initial guide to further refine the target on other MRI scans (Fig. 2). In fact, our group employed the 3T SWI sequence to identify STN-SNr borders on coronal and sagittal planes and then refined the target on the axial plane also with the aid of the more commonly employed T2* and FLAIR sequences. In our opinion, this two-step targeting process may overcome some limitations from previous studies, i.e. using 1.5.T SWI and considering only the axial plain while evaluating STN borders with SWI.[19,20] After identifying the STN-SNr border, it is also easier to locate on the axial plane the medial STN border, which is an important reference point to
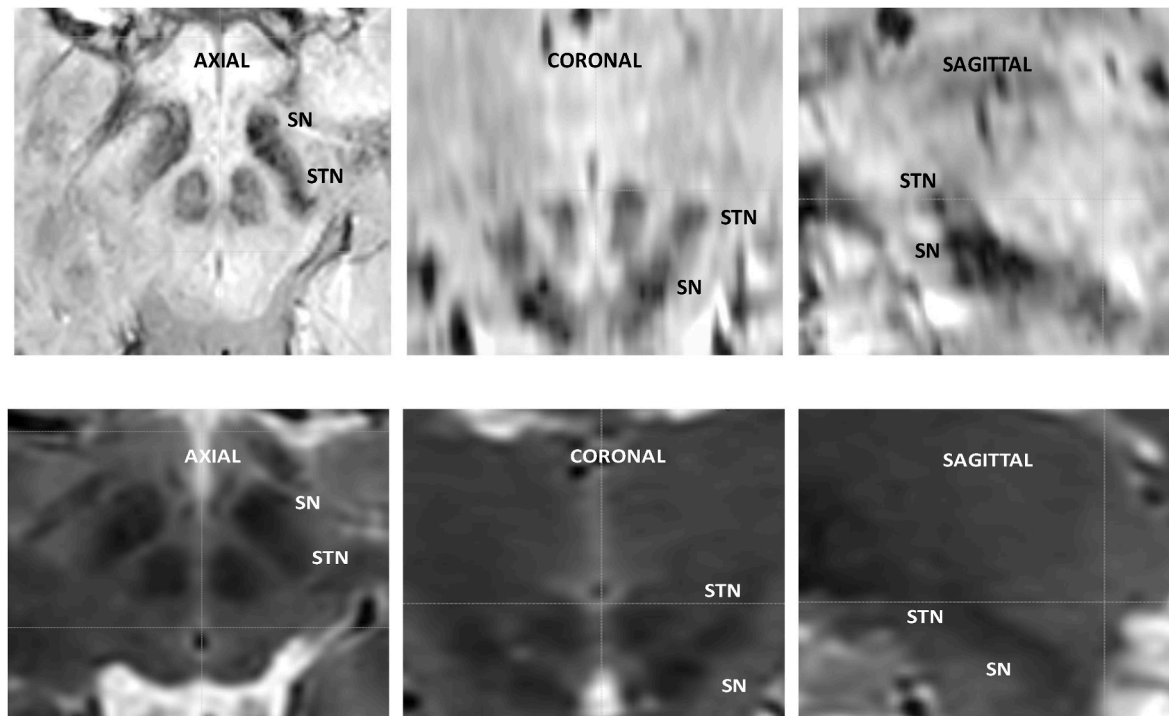
Fig. 2. Preoperative stereotactic planning of STN targeting on MRI 3T sequences.
For the same patient, note the better visualization of STN-SNr border when analyzing SWI sequences *(upper images)* rather than T2 ones *(lower images)*, especially in coronal and sagittal projections. STN = subthalamic nucleus. SN = substantia nigra.

locate the dorsolateral portion of STN.[32] The correct targeting of the dorsolateral portion of STN, roughly corresponding to its sensorimotor component, has a prominent clinical role: the sensorimotor STN (sm-STN) has wide connections to frontal and parietal sensorimotor cortices and suboptimal electrode positioning in associative and limbic STN subregions may elicit cognitive or emotional side effects during the stimulation.[33]

The main limitation of our study is the small size of the analyzed sample, which might have limited the relevance of certain parameters in the statistical analysis. For instance, the lower UPDRS III scores for the SWI-positive groups at one-year follow-up seem to suggest a possible clinical advantage for these patients, but this finding did not reach statistical significance and deserves further investigation. Finally, we judged statistical regression analyses as not feasible given the limited patient dataset. In fact, our study was designed as a preliminary study and further efforts are necessary to confirm and explore our findings.

5. Conclusions

To the best of our knowledge, this work is the first retrospective cohort study evaluating the efficacy of adding the SWI sequence to standard radiological protocols during the preoperative targeting in STN-DBS for Parkinson's disease. Despite the small sample size, we demonstrated the advantage of this strategy by proposing a two-step targeting method employing all three cartesian planes. We believe that further investigations on larger populations might show more convincing evidence confirming the reliability of the SWI sequence in clinical practice and the possible clinical advantages derived from adding this sequence to the preoperative MRI protocol.

CRediT authorship contribution statement

Luigi Gianmaria Remore: Conceptualization, Investigation, Methodology, Visualization, Writing – original draft, Writing – review & editing. **Leonardo Tariciotti:** Data curation, Formal analysis, Writing – review & editing. **Giorgio Fiore:** Methodology, Writing – review & editing. **Elena Pirola:** Writing – review & editing. **Linda Borellini:** Methodology, Writing – review & editing. **Filippo Cogiamanian:** Methodology, Writing – review & editing. **Antonella Maria Ampollini:** Writing – review & editing. **Luigi Schisano:** Writing – review & editing. **Dario Gagliano:** Writing – review & editing. **Stefano Borsa:** Writing – review & editing. **Mauro Pluderi:** Writing – review & editing. **Giulio Andrea Bertani:** Writing – review & editing. **Sergio Barbieri:** Writing – review & editing. **Marco Locatelli:** Project administration, Supervision, Writing – review & editing.

Declaration of competing interest

The authors declare that they have no known competing financial interests or personal relationships that could have appeared to influence the work reported in this paper.

References

1. Lee DJ, Lozano CS, Dallapiazza RF, Lozano AM. Current and future directions of deep brain stimulation for neurological and psychiatric disorders. *J Neurosurg.* 2019; 131(2):333–342. https://doi.org/10.3171/2019.4.JNS181761.
2. Schaltenbrand G. *Atlas for Stereotaxy of the Human Brain.* Georg Thieme; 1977. Published online.
3. Brunenberg EJL, Platel B, Hofman PAM, ter Haar Romeny BM, Visser-Vandewalle V. Magnetic resonance imaging techniques for visualization of the subthalamic nucleus: a review. *J Neurosurg.* 2011;115(5):970–984. https://doi.org/10.3171/2011.6.JNS101571.
4. O'Gorman RL, Shmueli K, Ashkan K, et al. Optimal MRI methods for direct stereotactic targeting of the subthalamic nucleus and globus pallidus. *Eur Radiol.* 2011;21(1):130–136. https://doi.org/10.1007/s00330-010-1885-5.
5. Lozano CS, Ranjan M, Boutet A, et al. Imaging alone versus microelectrode recording–guided targeting of the STN in patients with Parkinson's disease. *J Neurosurg.* 2019;1306(6):1847–1852. https://doi.org/10.3171/2018.2.JNS172186.
6. Remore LG, Omidbeigi M, Tsolaki E, Bari AA. Deep brain stimulation of thalamic nuclei for the treatment of drug-resistant epilepsy: are we confident with the precise surgical target? *Seizure.* 2023;105:22–28. https://doi.org/10.1016/j.seizure.2023.01.009.

7. Remore LG, Rifi Z, Nariai H, et al. Structural connections of the centromedian nucleus of thalamus and their relevance for neuromodulation in generalized drug-resistant epilepsy: insight from a tractography study. *Ther Adv Neurol Disord*. 2023; 16. https://doi.org/10.1177/17562864231202064.

8. Boutet A, Loh A, Chow CT, et al. A literature review of magnetic resonance imaging sequence advancements in visualizing functional neurosurgery targets. *J Neurosurg*. 2021;135(5):1445–1458. https://doi.org/10.3171/2020.8.JNS201125.

9. Boutet A, Gramer R, Steele CJ, et al. Neuroimaging technological advancements for targeting in functional neurosurgery. *Curr Neurol Neurosci Rep*. 2019;19(7). https://doi.org/10.1007/s11910-019-0961-8.

10. Melo M, Furlanetti L, Hasegawa H, Mundil N, Ashkan K. Comparison of direct MRI guided versus atlas-based targeting for subthalamic nucleus and globus pallidus deep brain stimulation. *Br J Neurosurg. Published online*. 2021. https://doi.org/10.1080/02688697.2020.1850641.

11. Abosch A, Yacoub E, Ugurbil K, Harel N. An assessment of current brain targets for deep brain stimulation surgery with susceptibility-weighted imaging at 7 tesla. *Neurosurgery*. 2010;67(6):1745–1756. https://doi.org/10.1227/NEU.0b013e3181f74105.

12. Chandran AS, Bynevelt M, Lind CRP. Magnetic resonance imaging of the subthalamic nucleus for deep brain stimulation. *J Neurosurg*. 2016;124(1):96–105. https://doi.org/10.3171/2015.1.JNS142066.

13. Gasparotti R, Pinelli L, Liserre R. New MR sequences in daily practice: susceptibility weighted imaging. A pictorial essay. *Insights Imaging*. 2011;2(3):335–347. https://doi.org/10.1007/s13244-011-0086-3.

14. di Ieva A, Lam T, Alcaide-Leon P, Bharatha A, Montanera W, Cusimano MD. Magnetic resonance susceptibility weighted imaging in neurosurgery: current applications and future perspectives. *J Neurosurg*. 2015;123(6):1463–1475. https://doi.org/10.3171/2015.1.JNS142349.

15. Mangia Pjt Silvia. Magnetic resonance imaging (MRI) in Parkinson's disease. *J Alzheimers Dis Parkinsonism*. 2013;3(3). https://doi.org/10.4172/2161-0460.s1-001.

16. McEvoy J, Ughratdar I, Schwarz S, Basu S. Electrophysiological validation of STN-SNr boundary depicted by susceptibility-weighted MRI. *Acta Neurochir*. 2015;157 (12):2129–2134. https://doi.org/10.1007/s00701-015-2615-1.

17. Vertinsky AT, Coenen VA, Lang DJ, et al. Localization of the subthalamic nucleus: optimization with susceptibility-weighted phase MR imaging. *Am J Neuroradiol*. 2009;30(9):1717–1724. https://doi.org/10.3174/ajnr.A1669.

18. Polanski WH, Martin KD, Engellandt K, et al. Accuracy of subthalamic nucleus targeting by T2, FLAIR and SWI-3-Tesla MRI confirmed by microelectrode recordings. *Acta Neurochir*. 2015;157(3):479–486. https://doi.org/10.1007/s00701-014-2328-x.

19. Bot M, Bour L, de Bie RM, Contarino MF, Schuurman PR, van den Munckhof P. Can we rely on susceptibility-weighted imaging for subthalamic nucleus identification in deep brain stimulation surgery? *Neurosurgery*. 2016;78(3):353–359. https://doi.org/10.1227/NEU.0000000000001130.

20. Bus S, van den Munckhof P, Bot M, et al. Borders of STN determined by MRI versus the electrophysiological STN. A comparison using intraoperative CT. *Acta Neurochir*. 2018;160(2):373–383. https://doi.org/10.1007/s00701-017-3432-5.

21. Urbaniak GC, Plous S. Research randomizer. http://www.randomizer.org/; June 22, 2013. Accessed December 19, 2021. https://www.randomizer.org/about/. Published.

22. Horn A, Li N, Dembek TA, et al. Lead-DBS v2: towards a comprehensive pipeline for deep brain stimulation imaging. *Neuroimage*. 2019;184:293–316. https://doi.org/10.1016/j.neuroimage.2018.08.068.

23. Horn A, Kühn AA. Lead-DBS: a toolbox for deep brain stimulation electrode localizations and visualizations. *Neuroimage*. 2015;107:127–135. https://doi.org/10.1016/j.neuroimage.2014.12.002.

24. Avants BB, Tustison NJ, Song G, Cook PA, Klein A, Gee JC. A reproducible evaluation of ANTs similarity metric performance in brain image registration. *Neuroimage*. 2011;54(3):2033–2044. https://doi.org/10.1016/j.neuroimage.2010.09.025.

25. Fonov V, Evans AC, Botteron K, Almli CR, McKinstry RC, Collins DL. Unbiased average age-appropriate atlases for pediatric studies. *Neuroimage*. 2011;54(1):313–327. https://doi.org/10.1016/j.neuroimage.2010.07.033.

26. Avants BB, Epstein CL, Grossman M, Gee JC. Symmetric diffeomorphic image registration with cross-correlation: evaluating automated labeling of elderly and neurodegenerative brain. *Med Image Anal*. 2008;12(1):26–41. https://doi.org/10.1016/j.media.2007.06.004.

27. Friston K, Holmes A, Worsley K, Poline J p, Frith C, Frackowiak R. *Statistical Parametric Maps in Functional Imaging: A General Linear Approach*. vol. 2. 1995.

28. Ewert S, Horn A, Finkel F, Li N, Kühn AA, Herrington TM. Optimization and comparative evaluation of nonlinear deformation algorithms for atlas-based segmentation of DBS target nuclei. *Neuroimage*. 2019;184:586–598. https://doi.org/10.1016/j.neuroimage.2018.09.061.

29. Husch A, Petersen M v, Gemmar P, Goncalves J, Hertel F. PaCER - a fully automated method for electrode trajectory and contact reconstruction in deep brain stimulation. *Neuroimage Clin*. 2018;17:80–89. https://doi.org/10.1016/j.nicl.2017.10.004.

30. Ewert S, Plettig P, Li N, et al. Toward defining deep brain stimulation targets in MNI space: a subcortical atlas based on multimodal MRI, histology and structural connectivity. *Neuroimage*. 2018;170:271–282. https://doi.org/10.1016/j.neuroimage.2017.05.015.

31. Mameli F, Ruggiero F, Dini M, et al. Energy delivered by subthalamic deep brain stimulation for Parkinson disease correlates with depressive personality trait shift. *Neuromodulation. Published online*. 2022. https://doi.org/10.1016/j.neurom.2022.01.004.

32. Bot M, Schuurman PR, Odekerken VJJ, et al. Deep brain stimulation for Parkinson's disease: defining the optimal location within the subthalamic nucleus. *J Neurol Neurosurg Psychiatry*. 2018;89(5):493–498. https://doi.org/10.1136/jnnp-2017-316907.

33. van Wijk BCM, Alkemade A, Forstmann BU. Functional segregation and integration within the human subthalamic nucleus from a micro- and meso-level perspective. *Cortex*. 2020;131:103–113. https://doi.org/10.1016/j.cortex.2020.07.004.